



Article

Effect of the Bionic Transverse Stripe on Wear Resistance and Crushing Performance of Cement Grinding Roller

Tingkun Chen ¹, Lin Wang ², Jin Xu ¹, Xiuzhang Qin ¹, Xinju Dong ¹, Qingbo Wang ¹, Yingchun Qi ¹, Jingfu Jin ¹, Qian Cong ^{1,*} and Chaozong Liu ³

¹ College of Biological and Agricultural Engineering, Key Laboratory of Bionic Engineering (Ministry of Education), Jilin University, Changchun 130022, China

² State Key Laboratory of Power Systems of Tractor, YTO Group Corporation, Luoyang 471039, China

³ Department of Ortho and MSK Science, University College London, London HA7 4LP, UK

* Correspondence: congqian@jlu.edu.cn

Abstract: To improve the wear resistance and mineral crushing performance of grinding rollers in cement, mining, and other engineering fields, a striped groove morphology was designed on the normal grinding roller surface in this study. The wear resistance of grinding rollers with different striped groove parameters and the crushing performance of quartz sand were tested with a purposely designed device. The depth and number of striped grooves were used as the structural parameters of the striped grooves, and the test protocol was designed with the experimental design method. The results showed that the wear resistance and crushing performance of the grinding roller with striped grooves were better than those of the smooth grinding roller for quartz sand. For example, the wear of the 3# bionic grinding roller was reduced by 53.58% compared with the average wear amount of a normal grinding roller, and the crushing effect of the quartz sand was also improved. The regression equation between the stripe depth, number of stripes, and wear amount of the grinding roller was constructed on the basis of the multiple orthogonal regression method. It was found that the influence of the striped groove depth on the wear amount of the grinding roller was greater than that of the distribution number of the striped grooves. According to the results and the analysis the striped grooves distributed on the grinding roller's surface caused the friction state between the quartz sand and the grinding roller to be in a state of sliding friction, and the wear amount was reduced. Striped grooves on the grinding roller surface might also change the stress state of the quartz sand in the crushing process. Additionally, the performance of the bionic grinding roller in crushing quartz sand was improved, and the wear amount of the bionic grinding roller was also reduced compared with that of the normal grinding roller.

Keywords: bionic; stripe; cement grinding roller; wear; crushing



Citation: Chen, T.; Wang, L.; Xu, J.; Qin, X.; Dong, X.; Wang, Q.; Qi, Y.; Jin, J.; Cong, Q.; Liu, C. Effect of the Bionic Transverse Stripe on Wear Resistance and Crushing Performance of Cement Grinding Roller. *Machines* **2023**, *11*, 239. <https://doi.org/10.3390/machines11020239>

Academic Editor: Francisco J. G. Silva

Received: 9 January 2023

Revised: 2 February 2023

Accepted: 2 February 2023

Published: 6 February 2023



Copyright: © 2023 by the authors. Licensee MDPI, Basel, Switzerland. This article is an open access article distributed under the terms and conditions of the Creative Commons Attribution (CC BY) license (<https://creativecommons.org/licenses/by/4.0/>).

1. Introduction

China is a large developing country and is in the process of industrialization and urbanization. A large amount of infrastructure construction in China is carried out every year. To carry out large-scale infrastructure construction, a large cement supply is required. According to statistics from reference [1], the annual production of cement in China exceeds 2 billion tons.

In the process of cement production, minerals need to go through several grinding processes before forming cement. As a kind of grinding equipment, the roller mill applies static high pressure on minerals to crush them. Hence, the roller mill is widely used in cement, mining, the chemical industry, and other fields [2,3]. In addition, most of the energy consumption in mining and mineral processing, about 75% to 85%, is used for grinding minerals [3,4]. However, the squeezing action of the minerals leads to an increase in the wear of the grinding rollers, reducing the efficiency of the mineral crushing and increasing

both equipment maintenance and production costs [5,6]. In addition, the abrasion of the grinding roller accounts for approximately 15–25% of the production costs [7].

Therefore, researchers are committed to developing methods that can improve the wear resistance of grinding rolls, such as improving the hardness of the grinding roller material, applying a wear-resistant coating and overlay welding, etc. [6,8–18]. Adetunji et al. [8] found that the wear resistance of grinding rolls could be improved by adding chromium and molybdenum to the grinding roller material. Li et al. [13] improved the hardness and strength of the grinding roller material by adjusting the heat treatment process of high-vanadium alloy steel, and the results showed that the wear resistance of the material increased. Some researchers have developed various processes to prepare wear-resistant coatings; for example, Tan et al. [17] prepared an AlZnCu amorphous coating by laser cladding. Due to the complexity and high cost of the coating preparation process, it cannot be applied in engineering [5,19]. Hence, the surface of grinding rollers is often hardened using weld-filling and hard-facing methods to improve the wear resistance and service life of grinding rollers. However, the surface of grinding rollers treated with the welding method is peeled off in a large area after long-term use, which is fatal to grinding rollers that apply high pressure to crush minerals.

After thousands of years of evolution, organisms in nature have formed the best body surface structure to adapt to their living environments. Researchers have begun to study the surface morphology of living organisms in nature, such as that of the dung beetle, desert scorpion, tamarisk, and boa, to enhance the wear resistance of components [20–29]. Ren et al. [25,26] prepared bionic pits on a bulldozer blade surface based on the head morphology of the dung beetle, which improved its service life and wear resistance. Abdel and Mansori [20] studied the scale surface morphology of python scales and pointed out that the scales had significant wear resistance. Cuervo et al. [21] designed a bionic texture on the surface of a titanium alloy according to the shape of the surface of snake scales, which reduced the friction coefficient of ultra-high molecular weight polyethylene on the sample surface. Yin et al. [28] studied the surface morphology of tamarisk leaves and designed a bionic sample with a grooved structure on the surface. Testing showed that the bionic samples had excellent wear resistance compared with conventional specimens. Han et al. [22–24] designed a wear-resistant surface according to the shape of the desert scorpion and dung beetle shell. For example, compared with the wear resistance of the smooth sample, the wear resistance of the bionic groove and the bionic bump increased by approximately 10% and 25%, respectively [24].

Shells are the outer shells of mollusks living in rivers and lakes and on seashores. After a long period of natural evolution, shell surfaces have formed non-smooth morphology to withstand the erosion of water and sediment [30]. Therefore, the non-smooth morphology of the shell surface was prepared on the grinding roller surface in the present study. The purposely designed device was used to test the wear resistance of the bionic grinding roller and the influence of the bionic grinding roller on the crushing performance of the sand, and the influence mechanism of the bionic morphology on the wear resistance of the grinding roller was analyzed. The present study could provide help for the development of grinding rollers with high abrasion resistance and crushing properties in the engineering field.

2. Materials and Methods

2.1. Grinding Roller Design

The test aimed to study the effect of the striped groove morphology on the performance of the grinding roller, and 45 steel is a common material used in engineering. Hence, 45 steel was selected as the material for the normal and bionic grinding roller. The length of the grinding roller was 250 mm, and the inner diameter and outer diameter were 130 mm and 150 mm, respectively. Rectangular slots were machined into the ends of the grinding roller for easy installation and performance testing, as shown in Figure 1.

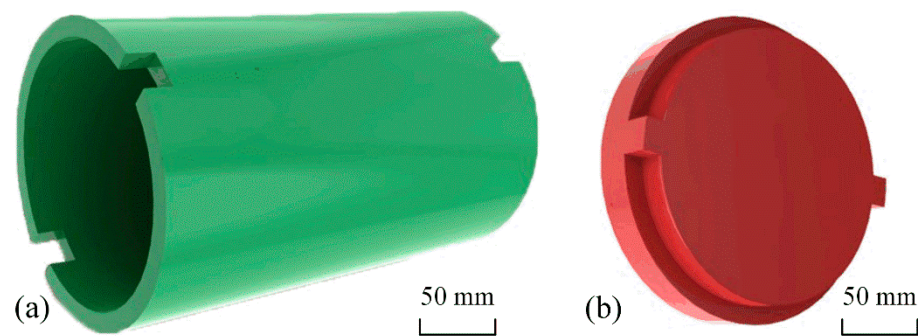


Figure 1. Grinding roller and holder. (a) model of the grinding roller; (b) fixture of the grinding roller.

During the test, the striped morphology of the shell surface was used as the design model, and the striped non-smooth structure was selected as the design morphology of the grinding roller surface. The depth and number of stripes were selected as the factors of the stripe texture, and the stripe pattern was uniformly distributed around the circumference of the grinding roller surface. The level values of the designed factors are shown in Table 1.

Table 1. Factors and levels table of the bionic grinding roller.

Levels	Factors	Depth of Stripe <i>D</i> /mm	Number of Stripes <i>N</i>
1		0.6 (1)	60 (1)
2		0.8 (2)	70 (2)
3		1.0 (3)	80 (3)

The test plan was complied with by using the L_9 (3^4) orthogonal table based on reference [31], shown in Table 2. Based on the smooth grinding roller shown in Figure 1, the bionic grinding roller with different parameters shown in Table 2 was processed by using the numerical control processing method.

Table 2. Factor, level, and test number.

Test No.	<i>D</i> (mm)	<i>N</i>	Test No.	<i>D</i> (mm)	<i>N</i>
1	1 (0.6)	1 (60)	6	2 (0.8)	3 (80)
2	1 (0.6)	2 (70)	7	3 (1.0)	1 (60)
3	1 (0.6)	3 (80)	8	3 (1.0)	2 (70)
4	2 (0.8)	1 (60)	9	3 (1.0)	3 (80)
5	2 (0.8)	2 (70)	Normal grinding roller		

2.2. Experiment Device

Based on the operation principle of a large grinding roller machine in the cement industry, a test device was developed to test the wear resistance of the grinding rollers shown in Figure 2. During the test, the grinding roller and fixture shown in Figure 1 were installed in the grinding roller support box, and the coupling was used to connect the grinding roller to the motor. The rotation direction of the two grinding rollers was opposite and inward on the drive of the motor (model size: Y 802-4, purchased from Shanghai Lidong Jidian Co., Ltd., Shanghai, China), as shown in Figure 2. The quartz sand was poured down above the middle area of the two grinding rollers. The crushed quartz sand fell into the sandbox under the crushing of the grinding roller. During the test, grinding rollers with different parameters could be replaced by removing the fixture of the grinding roller.

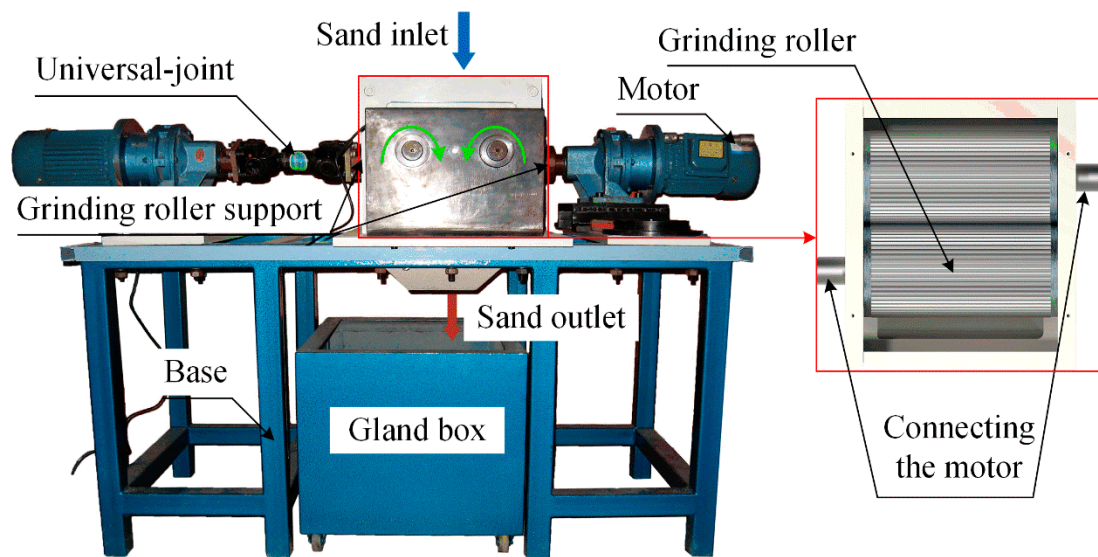


Figure 2. Experimental device.

2.3. Experiment Methods

2.3.1. Wear Test

Currently, there are several main methods to determine the amount of material wear, such as the weight loss method, the dimensional change method, the abrasive chip analysis method, etc. [32]. The weight loss method, which determines the wear amount by measuring the sample before and after the wear test with a precision electronic balance, is easy to perform and has high accuracy. Hence, the weight loss method was used to measure the wear of the sample during the test.

When the wear test of the grinding roller was carried out, the electronic balance was used to measure the initial weight of the grinding roller, and the device shown in Figure 2 was used to perform the wear resistance test. During the wear tests, 150 kg of quartz sand was used for each grinding roller with different parameters. When 150 kg of quartz sand was recycled four times, two grinding rollers were removed. The dust on the grinding roller surface was cleaned by using the brush and air jet to reduce the error. The weight of the two grinding rollers was measured. The difference in the average weight between the two rollers before and after the test was used as the test evaluation standard. The maximum range of the high-precision electronic balance (model size: GB 1202, purchased from Shinko Denshi Co., Ltd., Tokyo, Japan) was 20 kg, and the accuracy was ± 0.01 g.

2.3.2. Crushing Test

In the experiment, the effect of the stripe morphology on the wear resistance of the grinding rollers was tested, along with the crushing effect on the quartz sand. The higher the mass of fine quartz sand after crushing, the finer the quartz sand was crushed, and the better the grinding roller crushed the quartz sand. Therefore, a sieve with a pore size of 5 mm commonly used in the construction industry was used in the experiment to screen out large-grain quartz sand with a mass of about 6 kg during the test. The effect of grinding rollers with different striping parameters on the crushing effect of the quartz sand was carried out using the experimental apparatus shown in Figure 2. The crushing was carried out six times. Quartz sand with different particle sizes after each crushing was screened separately using the sieve shown in Figure 3, and the mass ratio of each different particle size of quartz sand was calculated by equation 1. In the test, the minimum diameters of the five sieves were 5 mm, 4 mm, 2 mm, 1 mm, and 0.5 mm, respectively, as shown in Figure 3.

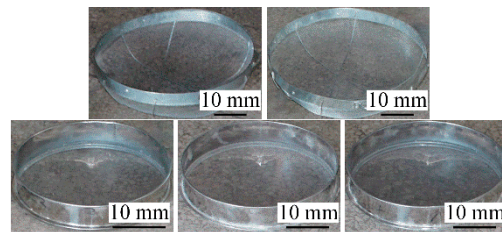


Figure 3. Sieves for screening sand during the test.

The certain particle size grade was calculated as follows:

$$\lambda_n = \frac{B_n}{A} \times 100\% \quad (1)$$

where λ_n and B_n are the mass and ratio of gravel, respectively; A is the initial mass of quartz sand (approximately 6 kg).

3. Results

3.1. Wear Tests

According to the test protocol prepared for the experiment, the wear tests of the bionic and conventional grinding rollers were conducted by the device shown in Figure 2. Figure 4 shows the grinding roller after several wear tests.

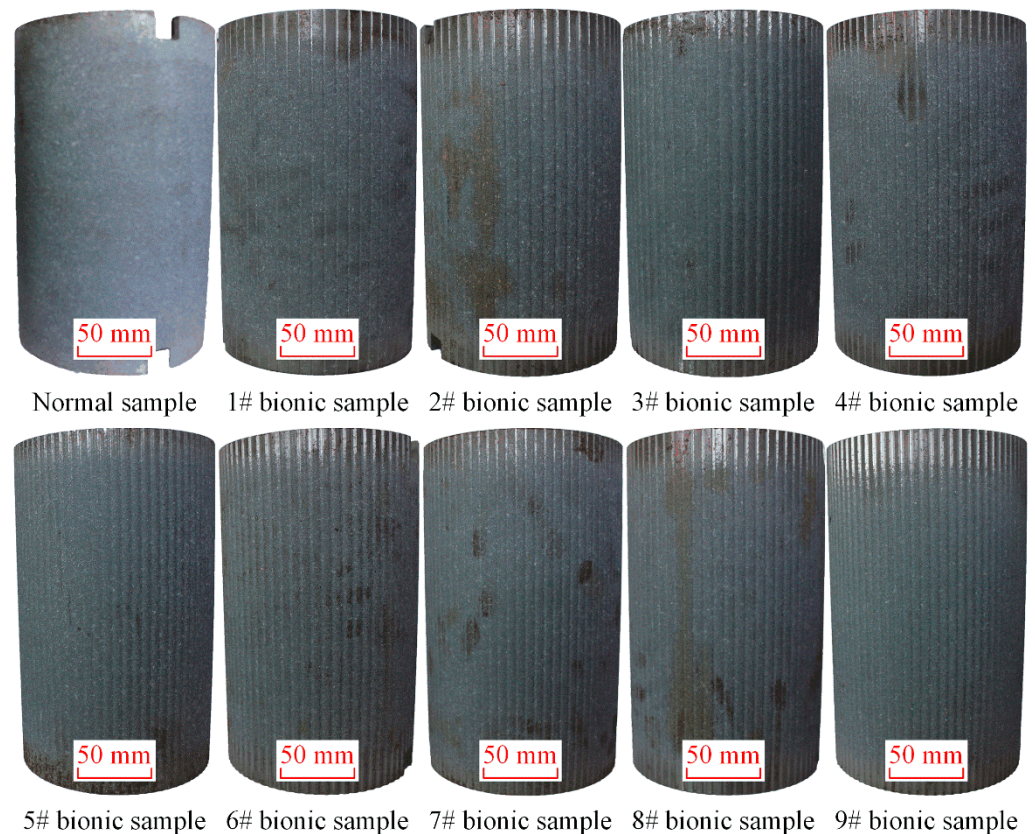


Figure 4. Worn grinding rollers.

According to the prepared test program L_9 (3^4), the average wear amounts of the different grinding rollers are shown in Table 3. After four times of the wear test, the average wear amount of the smooth grinding roller was 4.89 g. It was seen that grinding rollers with striped groove morphology showed a reduced wear amount compared with the average wear of a smooth grinding roller. During the wear test, the 3# and 6# bionic grinding

rollers had the smallest and largest wear amounts, respectively. The average wear amount of the 3# bionic grinding roller reached 2.27 g. The results for the different parameters of the grinding rollers in Table 3 were subjected to extremum difference analysis. It was determined that the effect of factor B on the amount of wear was less than that of factor A. In addition, when the depth and number of stripes were 0.6 mm and 80, respectively, the wear amount was reduced to the minimum. This was consistent with the design parameters of the 3# bionic grinding roller.

Table 3. Range analysis of wear test of the bionic grinding roller.

Test No.	A Stripe Depth	B Number of Stripes	Average Wear Amount/g
1	1 (0.6)	1 (60)	3.745
2	1 (0.6)	2 (70)	3.53
3	1 (0.6)	3 (80)	2.27
4	2 (0.8)	1 (60)	2.41
5	2 (0.8)	2 (70)	3.485
6	2 (0.8)	3 (80)	3.97
7	3 (1.0)	1 (60)	2.305
8	3 (1.0)	2 (70)	2.41
9	3 (1.0)	3 (80)	3.5
\bar{y}_{j1}	2.65	3.92	
\bar{y}_{j2}	3.29	3.18	
\bar{y}_{j3}	2.74	2.91	
R_j	0.64	0.27	
Primary and secondary factors	A	B	
Optimal combination	A ₁ B ₃		

The extremum difference analysis method was used to determine the best design parameters of the stripe morphology, and the value of the designed factors of the striped grooves was discrete. It was impossible to analyze the influence of the trend of factors on the test indexes. Therefore, on the basis of the prepared test scheme and the results in Table 3, the multivariate orthogonal polynomial method was used to conduct a regression analysis on the experimental results to explore the influence of factors on the experimental indicators [31].

The regression coefficients of the regression equation between the factors and indicators of the test were obtained, as shown in Table 4, and whether the regression coefficients were significant was determined. If the regression coefficient α_j was greater than 0.1, the relative factor was insignificant and the influence of the factor on the test indicator was not significant, and it was not considered when determining the regression equation [31]. For example, since the regression coefficient α_j of $X_2 (Z_1)$ was 0.25, the effect of $X_2 (Z_1)$ on the wear amount of the grinding roller was not considered, and it was removed when constructing the regression equation.

Table 4. Results of the regression coefficient.

	$X_1 (Z_1)$	$X_2 (Z_1)$	$X_1 (Z_2)$	$X_2 (Z_2)$	$X_1 (Z_1) * X_1 (Z_2)$	$X_1 (Z_1) * X_2 (Z_2)$	$X_2 (Z_1) * X_1 (Z_2)$	$X_2 (Z_1) * X_2 (Z_2)$
b_j	-0.2217	-0.1094	0.2133	-0.0361	0.6675	0.1692	-0.2833	0.0311
S_j	0.2948	0.2156	0.2731	0.0235	1.7822	0.3434	0.9633	0.0348
F_j	10.1109	7.3943	9.3650	0.805	61.1223	11.7774	33.038	1.195
α_j	0.1	0.25	0.1	0.25	0.01	0.1	0.05	0.25

Note: “ $X_1 (Z_1)$ ” and “ $X_2 (Z_1)$ ” were the primary and secondary terms of the stripe depth in the regression analysis, respectively. “ $X_1 (Z_1) * X_1 (Z_2)$ ” was the interaction between the stripe depth and the number of stripes.

On the basis of the results calculated in Table 4, the regression equation between factors and test indicators in the coding space was determined, as shown in Equation (2).

$$Y = 3.0694 - 0.2217X_1(Z_1) - 0.1094X_2(Z_1) + 0.2133X_1(Z_2) + 0.6675X_1(Z_1)X_1(Z_2) + 0.1692X_1(Z_1)X_2(Z_2) - 0.2833X_2(Z_1)X_1(Z_2) \quad (2)$$

The regression test and misfit test were performed on Equation (2) by Equation (3). The results showed that Equation (2) had good significance and did not fit.

$$\begin{cases} F_{regression} = \frac{S_{regression} / f_{regression}}{S_{residual} / f_{residual}} \\ \beta_{residual} = \frac{S_{residual}}{S} \end{cases} \quad (3)$$

Here, $S_{regression}$ and $S_{residual}$ are the residual sum of squares and the regression sum of squares, and $f_{regression}$ and $f_{residual}$ are their degrees of freedom, respectively. S is the total sum of squares.

According to reference [31], Equation (2) was transformed into a regression equation of factors and indicators in natural space by combining Equation (4).

$$\begin{cases} X_1(Z_1) = \lambda_1 \frac{z_1 - \bar{z}_1}{\Delta_1} = 5z_1 - 4 \\ X_2(Z_1) = \lambda_2 \left[\left(\frac{z_1 - \bar{z}_1}{\Delta_1} \right)^2 - \frac{N^2 - 1}{12} \right] = 75z_1^2 - 120z_1 + 46 \\ X_1(Z_2) = \lambda_1 \frac{z_2 - \bar{z}_2}{\Delta_2} = 0.1z_2 - 7 \\ X_2(Z_2) = \lambda_2 \left[\left(\frac{z_2 - \bar{z}_2}{\Delta_2} \right)^2 - \frac{N^2 - 1}{12} \right] = 0.03z_2^2 - 4.2z_2 + 145 \end{cases} \quad (4)$$

During the test, the regression equation between the factors and the test index was shown in Equation (5):

$$A = 9.207 - 126.645x - 1.294y + 140.528x^2 - 0.02y^2 + 0.18xy + 0.025xy^2 - 2.12x^2y \quad (5)$$

Here, x , and y represented the depth and number of the stripes; A is the wear amount of the grinding roller.

Figure 5 shows the response surface between the factors and the test index. It was seen that the wear amount of the grinding roller gradually increased and then gradually decreased with the increase in the stripe depth. However, when the number of striped grooves increased, the effect of the stripe depth on wear changed, as shown in Figure 5. The wear amount of the grinding roller gradually increased and then gradually decreased with the increase in the number of striped grooves. However, this trend was not obvious when the number of striped grooves was below 70. It can be seen from the trend of the wear amount in Figure 5 that the number of striped grooves and the striped groove depth had an interactive effect on the wear amount of the grinding roller. This can also be seen in Equation (5).

3.2. Crushing Tests

The grade of the crushed quartz sand is shown in Figure 6. The quartz sand was gradually refined with the increase in the number of crushing times. In the test, the quality of grade 6 quartz sand was used as the evaluation standard of the grinding roller crushing effect.

Figure 7 shows the effect of bionic grinding rollers with different stripe parameters on the crushing effect of the quartz sand. It can be seen in Figure 7 that the grade 2 quartz sand had the largest mass proportion, and the grade 5 quartz sand had the smallest mass proportion. When the crushed quartz sand grade was 6, the crushing effect of the grinding roller with the striped morphology was better than that of the smooth grinding roller. Among them, the 3# bionic grinding roller had the best crushing performance on the quartz sand.

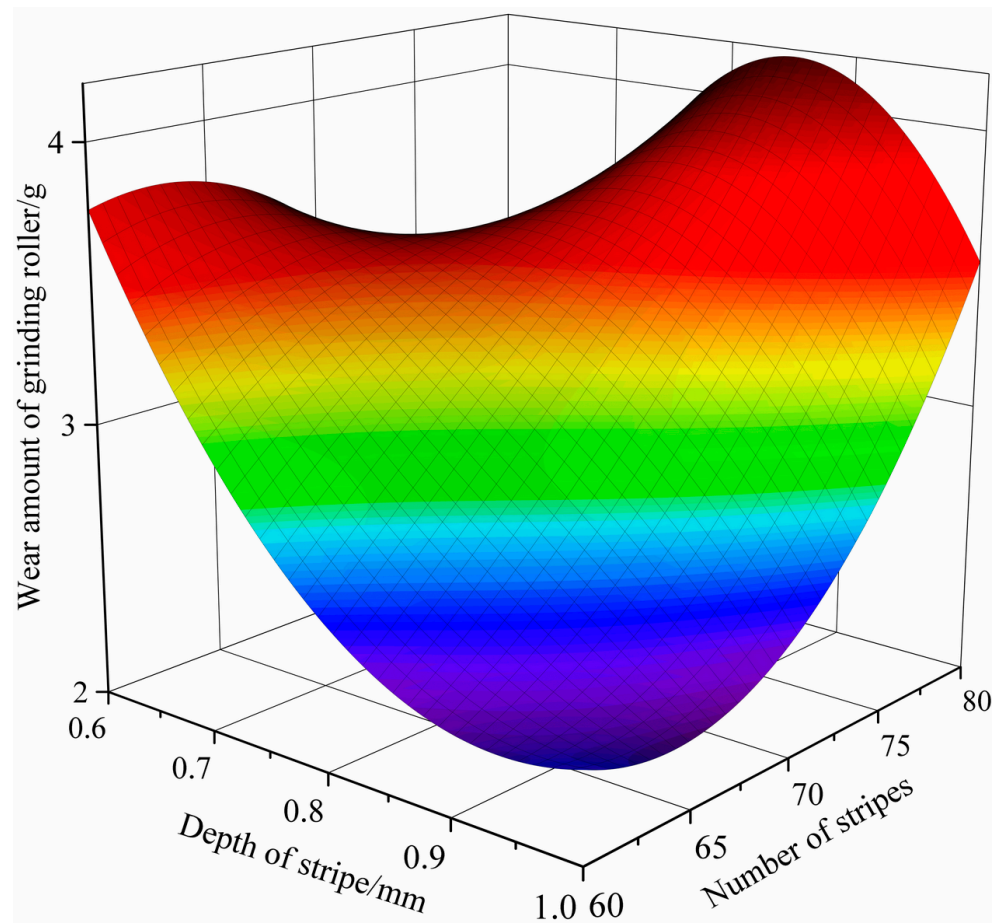


Figure 5. Effect of stripe depth and the number of stripes on wear performance of grinding rollers.



Grade of particle size: 1



Grade of particle size: 2



Grade of particle size: 3



Grade of particle size: 4



Grade of particle size: 5



Grade of particle size: 6

Figure 6. Particle size grade after abrasion.

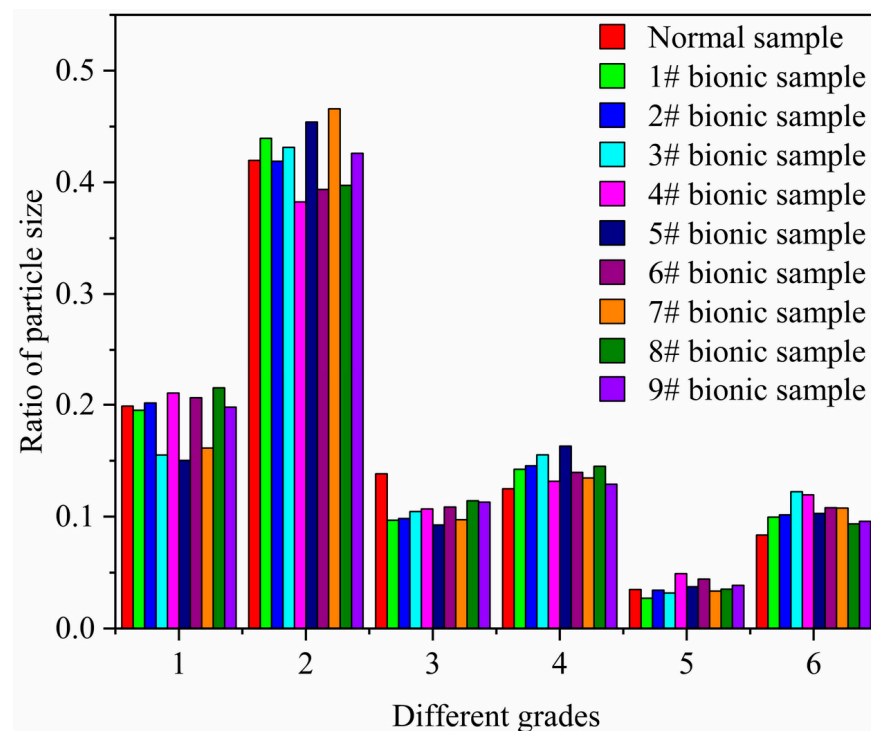


Figure 7. The effect of different grinding rollers on crushing sand.

4. Discussion

From the test results shown in Table 3 and Figure 7, it can be seen that compared with the smooth grinding rollers, the grinding rollers with striped morphology had good wear resistance and a good crushing effect on the quartz sand. The striped groove morphology on the grinding roller surface changed the sliding state of the quartz sand between the two grinding rollers, as shown in Figure 8. When the quartz sand was crushed between two smooth grinding rollers, the quartz sand was in a sliding friction state between the two smooth grinding rollers due to the absence of macroscopic morphology on the grinding roller's surface, as shown in Figure 8a. This easily caused the quartz sand to scratch the grinding roller surface and increased the wear amount of the grinding roller caused by the quartz sand. Meanwhile, it reduced the crushing effect of the grinding roller on the quartz sand.

When there were striped grooves on the grinding roller surface, the edge of the striped grooves and the irregular shape of the quartz sand made it difficult for the quartz sand to slide on the grinding roller surface. This changed the friction state between the quartz sand and the grinding roller. Therefore, it was considered that the contact state between the quartz sand and the bionic grinding roller was rolling, as shown in Figure 8b. When the number of striped grooves was large, it was easy to make contact between the quartz sand and the grinding roller in a rolling state. When the striped groove depth was small, the irregular quartz sand more easily contacted the bottom of the striped groove, which made it easier for the quartz sand to be in a rolling state during the crushing process. The scratching of quartz sand on the grinding roller surface was reduced, and the wear amount of the quartz sand on the bionic grinding roller was reduced. Therefore, it can be approximately considered that the striped grooves on the grinding roller surface changed the sliding state between the quartz sand and the grinding roller.

The striped grooves on the grinding roller surface could change the frictional state between the quartz sand and the grinding roller surface, as well as the stress state of the quartz sand in the crushing process, as shown in Figure 9. The smooth grinding roller surface was in single-point contact with the quartz sand, and the force acted directly on one point of the grinding roller surface. During the crushing process, the quartz sand contacted

the grinding roller surface with striped grooves at multiple points. The force was separated into several small forces, reducing the stress on the grinding roller and decreasing the wear amount of the grinding roller. The quartz sand could not contact the bottom surface of the striped grooves of the grinding roller with the increase in the grinding roller depth, as shown in Figure 9b. This increased the force between the quartz sand and both sides of the striped groove and reduced the crushing effect of the bionic grinding roller on the quartz sand. When the groove depth of the grinding roller was reduced, the quartz sand could be in contact with the bottom surface of the striped grooves of the grinding roller so that more squeezing force was applied to the quartz sand, as shown in Figure 9c. The quartz sand could be easily crushed, and the wear amount of the grinding roller was reduced.

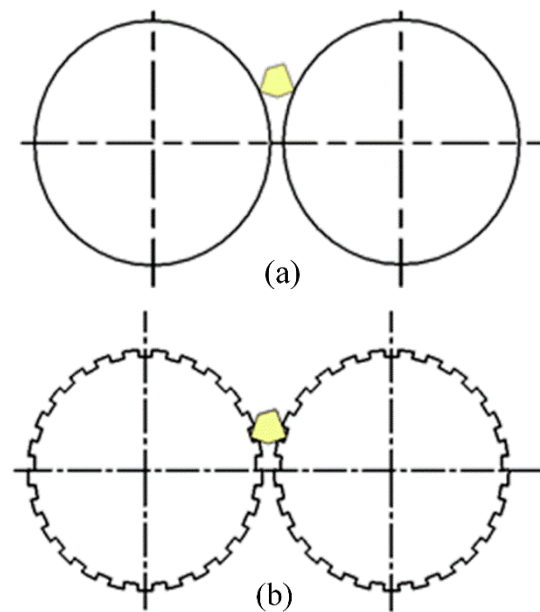


Figure 8. Rolling the quartz sand between different grinding rollers. (a) normal grinding roller (b) bionic grinding roller.

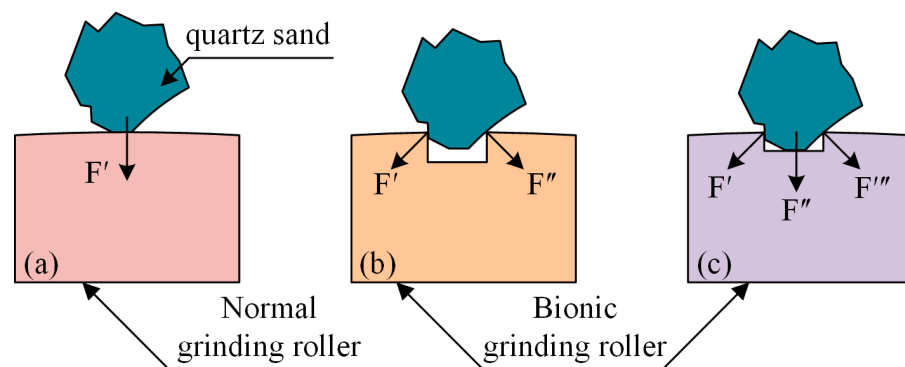


Figure 9. The influence of different contact interfaces on the forces of sand. (a) contact between quartz sand and grinding roller; (b) contact between quartz sand and the bionic grinding roller with the deeper groove; (c) contact between quartz sand and the bionic grinding roller with a smaller depth groove.

5. Conclusions

It can be seen from the experimental results that compared with the average wear amount of the smooth grinding roller, the bionic grinding roller with striped grooves could significantly reduce the wear of the grinding roller in the crushing process.

The influence of striped groove depth on the average wear amount of the grinding roller was greater than that of the number of striped grooves. When the depth and number

of striped grooves on the grinding roller surface were 0.6 mm and 80, the average wear amount of the bionic grinding roller was 2.27 g. Compared with the average wear amount of a normal grinding roller, the average wear amount of the 3# bionic grinding roller was reduced by 53.58%. Meanwhile, the crushing test on the quartz sand showed that the grinding roller with striped grooves also improved the crushing performance on quartz sand.

It was concluded that the striped grooves on the grinding roller surface could change the friction state between the quartz sand and the grinding roller, and they could also change the stress state of the quartz sand in the crushing process. Therefore, the striped grooves on the grinding roller surface could improve the crushing effect on the quartz sand as well as reduce the wear amount during the test. The present study could help to provide a reference for the design of a grinding roller with wear resistance and good crushing of minerals in the engineering field, especially in the cement and mining industries.

Author Contributions: Conceptualization, T.C., L.W., J.X., X.Q., X.D., Y.Q. and Q.C.; methodology, T.C., L.W., Q.W., Y.Q., J.J., Q.C. and C.L.; validation, T.C., J.X., X.Q. and X.D.; formal analysis, T.C., L.W., Q.W., Y.Q., J.J. and C.L.; investigation, T.C., L.W. and Q.C.; resources, L.W. and Q.C.; data curation, T.C., J.X., X.Q., Q.W., Y.Q. and Q.C.; writing—original draft preparation, T.C. and X.D.; writing—review and editing, T.C., Q.C. and C.L.; visualization, T.C., J.X., X.Q., Q.W., Y.Q. and Q.C.; supervision, T.C. and Q.C.; project administration, T.C. All authors have read and agreed to the published version of the manuscript.

Funding: This research was supported by the State Key Laboratory of Power Systems of Tractor, China (Grant No. SKT2022002), and the National Natural Science Foundation of China (Grant No. 51205157).

Data Availability Statement: The data supporting the findings of this study are available in the article.

Conflicts of Interest: On behalf of all authors, the corresponding author states that there is no conflict of interest. The funder had no role in the test design, collection, analyses, or interpretation of data; the writing of the manuscript; or the decision to publish the results.

References

1. National Bureau of Statistics of China. *2020 China Statistical Yearbook*, 1st ed.; China Statistics Press: Beijing, China, 2020.
2. Maxton, D.; Morley, C.; Bearman, R. A quantification of the benefits of high pressure rolls crushing in an operating environment. *Miner. Eng.* **2003**, *16*, 827–838. [[CrossRef](#)]
3. Sesemann, Y.; Broeckmann, C.; Hoftler, A. A new laboratory test for the estimation of wear in high pressure grinding rolls. *Wear* **2013**, *302*, 1088–1097. [[CrossRef](#)]
4. Hosten, C.; Fidan, B. An industrial comparative study of cement clinker grinding systems regarding the specific energy consumption and cement properties. *Powder Technol.* **2012**, *221*, 183–188. [[CrossRef](#)]
5. Chang, S.; Pyun, Y.S.; Amanov, A. Wear enhancement of wheel-rail interaction by ultrasonic nanocrystalline surface modification technique. *Metals* **2017**, *10*, 188. [[CrossRef](#)] [[PubMed](#)]
6. Jensen, L.R.D.; Møller, P.; Jespersen, M. Corrosion of high chrome wear part materials used in vertical roller mills. *Corros. Eng. Sci. Technol.* **2011**, *46*, 790–795. [[CrossRef](#)]
7. Vermeulen, L.A.; Howat, D.D. Theories of ball wear and the results of a marked-ball test in ball milling. *J. S. Afr. Inst. Min. Metall.* **1983**, *83*, 189–197.
8. Adetunji, O.R.; Onawoga, D.T.; Adegbesan, O.O.; Dairo, O.U. Modification of steel roller composition to curb excessive wear. *J. Fail. Anal. Prev.* **2019**, *19*, 1655–1665. [[CrossRef](#)]
9. Chen, H.X.; Kong, D.J. Effects of laser remelting speeds on microstructure, immersion corrosion, and electrochemical corrosion of arc-sprayed amorphous Al-Ti-Ni coatings. *J. Alloys Compd.* **2019**, *771*, 584–594. [[CrossRef](#)]
10. Gao, M.H.; Lu, W.Y.; Yang, B.J.; Zhang, S.D.; Wang, J.Q. High corrosion and wear resistance of Al-based amorphous metallic coating synthesized by HVOF spraying. *J. Alloys Compd.* **2018**, *735*, 1363–1373. [[CrossRef](#)]
11. Henao, J.; Concustell, A.; Cano, I.G.; Dosta, S.; Cinca, N.; Guilemany, J.M.; Suhonen, T. Novel Al-based metallic glass coatings by cold gas spray. *Mater. Desig.* **2016**, *94*, 253–261. [[CrossRef](#)]
12. Jensen, L.R.D.; Fundal, E.; Moller, P.; Jespersen, M. Wear mechanism of abrasion resistant wear parts in raw material vertical roller mills. *Wear* **2011**, *271*, 2707–2719. [[CrossRef](#)]
13. Li, H.Z.; Tong, W.P.; Cui, J.J.; Zhang, H.; Chen, L.Q.; Zuo, L. Heat treatment of centrifugally cast high-vanadium alloy steel for high-pressure grinding roller. *Acta Metall. Sin. -Engl. Lett.* **2014**, *27*, 430–435. [[CrossRef](#)]

14. Lanzutti, A.; Novak, J.S.; De Bona, F.; Bearzi, D.; Magnan, M.; Fedrizzi, L. Failure analysis of cemented carbide roller for cold rolling: Material characterization, numerical analysis, and material modeling. *Eng. Fail. Anal.* **2020**, *116*, 104755. [[CrossRef](#)]
15. Suliga, M. The influence of the high drawing speed on mechanical-technological properties of high carbon steel wires. *Arch. Metall. Mater.* **2011**, *56*, 823–828. [[CrossRef](#)]
16. Suliga, M.; Kruzel, R. The mechanical properties of high carbon steel wires drawn in conventional and hydrodynamic dies. *Metallurgija* **2013**, *52*, 43–46.
17. Tan, C.L.; Zhu, H.M.; Kuang, T.C.; Shi, J.; Liu, H.W.; Liu, Z.W. Laser cladding Al-based amorphous-nanocrystalline composite coatings on AZ80 magnesium alloy under water cooling condition. *J. Alloys Compd.* **2017**, *690*, 108–115. [[CrossRef](#)]
18. Xiao, B.T.; Yan, X.F.; Jiang, W.M.; Fan, Z.T.; Huang, Q.W.; Fang, J.; Xiang, J.H. Comparative study on the hardness and wear resistance of the remelted gradient layer on ductile iron fabricated by plasma transferred arc. *Metals* **2022**, *12*, 644. [[CrossRef](#)]
19. Zhou, Z.D.; Zhang, Z.B.; Chen, Y.X.; Liang, X.B.; Shen, B.L. Composition optimization of Al-Ni-Ti alloys based on glass-forming ability and preparation of amorphous coating with good wear resistance by plasma spray. *Surf. Coat. Technol.* **2021**, *408*, 126800. [[CrossRef](#)]
20. Abdel-Aal, H.A.; Mansori, M.E. Tribological analysis of the ventral scale structure in a Python regius in relation to laser textured surfaces. *Surf. Topogr.-Metrol. Prop.* **2013**, *1*, 015001. [[CrossRef](#)]
21. Cuervo, P.; Lopez, D.A.; Cano, J.P.; Sanchez, J.C.; Rudas, S.; Estupinan, H.; Toro, A.; Abdel-Aal, H.A. Development of low friction snake-inspired deterministic textured surfaces. *Surf. Topogr.-Metrol. Prop.* **2016**, *4*, 024013. [[CrossRef](#)]
22. Han, Z.W.; Xu, X.X.; Qiu, Z.M.; Ren, L.Q. Investigation of micro-wear and micro-friction properties for bionic non-smooth concave components. *J. Bionic Eng.* **2005**, *2*, 63–67. [[CrossRef](#)]
23. Han, Z.W.; Mu, Z.Z.; Yin, W.; Li, W.; Niu, S.C.; Zhang, J.Q.; Ren, L.Q. Biomimetic multifunctional surfaces inspired from animals. *Adv. Colloid. Interface Sci.* **2016**, *234*, 27–50. [[CrossRef](#)]
24. Han, Z.W.; Zhu, B.; Yang, M.K.; Niu, S.C.; Song, H.L.; Zhang, J.Q. The effect of the micro-structures on the scorpion surface for improving the anti-erosion performance. *Surf. Coat. Technol.* **2017**, *313*, 143–150. [[CrossRef](#)]
25. Ren, L.Q.; Han, Z.W.; Li, J.J.; Tong, J. Effects of non-smooth characteristics on bionic bulldozer blades in resistance reduction against soil. *J. Terramech.* **2002**, *39*, 221–230. [[CrossRef](#)]
26. Ren, L.Q.; Han, Z.W.; Li, J.J.; Tong, J. Experimental investigation of bionic rough curved soil cutting blade surface to reduce soil adhesion and friction. *Soil Tillage Res.* **2006**, *85*, 1–12. [[CrossRef](#)]
27. Wang, Z.Z.; Gao, K.; Sun, Y.H.; Zhang, Z.H.; Zhang, S.Y.; Liang, Y.H.; Li, X.J.; Ren, L.Q. Effects of bionic units in different scales on the wear behavior of bionic impregnated diamond bits. *J. Bionic Eng.* **2016**, *13*, 659–668. [[CrossRef](#)]
28. Yin, W.; Han, Z.W.; Feng, H.L.; Zhang, J.Q.; Cao, H.N.; Tian, Y. Gas-solid erosive wear of biomimetic pattern surface inspired from plant. *Tribol. Trans.* **2017**, *60*, 159–165. [[CrossRef](#)]
29. Zhang, B.C.; Zhang, Z.Q.; Sun, J.W.; Shao, C. Design and wear resistance analysis of bionic roller for folding of automobile body cover parts based on pearl shell surface texture. *Surf. Topogr.-Metrol. Prop.* **2020**, *8*, 045027. [[CrossRef](#)]
30. Ren, L.Q.; Liang, Y.H. *The Introduction of Bionics*, 1st ed.; Science Press: Beijing, China, 2016.
31. Ren, L.Q. *Regression Design and Optimization*, 1st ed.; Science Press: Beijing, China, 2009.
32. Chang, K.H.; Choi, K.K. Error analysis and mesh adaptation method for shape design of structural components. *Comput. Struct.* **1992**, *44*, 1275–1289. [[CrossRef](#)]

Disclaimer/Publisher’s Note: The statements, opinions and data contained in all publications are solely those of the individual author(s) and contributor(s) and not of MDPI and/or the editor(s). MDPI and/or the editor(s) disclaim responsibility for any injury to people or property resulting from any ideas, methods, instructions or products referred to in the content.